Quantum Dynamics Simulations of Exciton Polariton Transport

Benjamin X. K. Chng,[†] M. Elious Mondal,[‡] Wenxiang Ying,[‡] and Pengfei Huo[*,‡,¶,§]

†*Department of Physics, University of Rochester, Rochester, New York, 14627, USA*
‡*Department of Chemistry, University of Rochester, Rochester, New York, 14627, USA*
¶*Institute of Optics, Hajim School of Engineering and Applied Sciences, University of Rochester, Rochester, New York, 14627, USA*
§*Center for Coherence and Quantum Optics, University of Rochester, Rochester, New York 14627, USA*

E-mail: pengfei.huo@rochester.edu

Abstract

Recent experiments have shown that exciton transport can be significantly enhanced through hybridization with confined photonic modes in a cavity. The light-matter hybridization generates exciton-polaritons bands, whose group velocity is significantly larger than the excitons. Dissipative mechanisms that affect the constituent states of EPs, such as exciton-phonon coupling and cavity loss, have been observed to reduce the group velocities in experiments. To elucidate the impacts of these dissipative mechanisms on polariton transport, we develop an efficient quantum dynamics approach that allows us to directly simulate polariton transport under the collective coupling regime and beyond long-wavelength approximation. Our numerical results suggest a renormalization of the group velocities with stronger exciton-phonon coupling strengths and a smaller Q-factor. We observe the transition from ballistic to diffusive propagation, as well as the quality factor-dependent behavior of the transient mean square displacement, agreeing well with the recent experimental measurements.

KEYWORDS: *Polariton Transport, Ballistic Motion, Exciton Polariton, Light-Matter Interactions, Quantum Electrodynamics Simulations, Group Velocity Renormalization*

Enabling efficient excitation energy transport is essential for basic energy science and device applications. However, the inherent disorders and exciton-phonon interactions within these materials restrict transport, resulting in slow, diffusive motion of exciton that constrains the device's performance. Recent experiments have demonstrated that exciton transport is significantly enhanced when they are strongly coupled to cavity modes.[1–5] This leads to large group velocities up to 40 μm ps^{-1} for halide perovskites in a Fabry-Pérot (FP) cavity[3] and up to 180 μm ps^{-1} for an organic semiconductor in a photonic crystal cavity[1] with micrometer range of transport. In Ref. 1 the polariton transport achieves 100 μm in 1 ps, enabling long-range energy transport.

Experiments reveal that the measured group velocities of molecular polaritons are lower than those predicted by their dispersion relations,[1–3,6] which is referred to as the renormalization of group velocity. Ultrafast measurements reported in Refs. 1 and 3 indicate more deviation from the predicted velocities with an increase in the wavepacket's excitonic character. These findings underscore the importance of phonon-mediated scattering in influencing polariton transport via its excitonic component. Additionally, Ref. 2 reports that the polariton wavepacket's velocities are strongly dependent on the cavity quality factor $\mathcal{Q}$, although $\mathcal{Q}$ is not related to the polariton's dispersion. The $\mathcal{Q}$-factor, which affects the polariton's lifetime, also correlates with the polariton's coherence lifetimes[7,8] and hence, its transport properties, including both transient mean-square displacement (MSD) and group velocities.

We examine the influence of various dissipative mechanisms on the transport properties of molecular polaritons in a FP cavity using the mean-field Ehrenfest (MFE) quantum dynamics method[9,10] to simulate the dynamics of the hybrid light-matter system. Notably, polariton transport occurs in a collective regime in which a substantial number of excitons (thousands or more) are resonantly coupled to cavity modes, resulting in upper polariton (UP) and lower polariton (LP) bands, as well as dark states that do not contain any significant photonic character. To faithfully model the transport process, one needs to consider at least $N = 10^4 - 10^6$ molecules and $\mathcal{M} = 10^2 - 10^4$ cavity modes (that satisfy the dispersion relation), presenting a significant computational challenge. Existing theoretical work either does not consider cavity loss[3] or is limited to the size of the system[7] in the transport simulations (such as only using $N = 512$ molecules and $\mathcal{M} = 160$ modes in Ref. 7).

We follow the previous work[3] and consider the generalized Holstein-Tavis-Cummings (GHTC) Hamiltonian[3,11–13]

$$\hat{H} = \hat{H}_{\mathrm{ex}} + \hat{H}_{\mathrm{ph}} + \hat{H}_{\mathrm{LM}} + \hat{H}_{\text{ex-b}} + \hat{H}_{\mathrm{b}}. \tag{1}$$

The fundamental assumption used in GHTC Hamiltonian (compared to the rigorous quantum electrodynamics Hamiltonian) can be found in Ref. 11 (see Sec. 2.6.1) as well as in Refs. 14–16. The excitonic Hamiltonian is $\hat{H}_{\mathrm{ex}} = \sum_{n=0}^{N-1}(\hbar\omega_{\mathrm{ex}} + \lambda)\hat{\sigma}_n^\dagger\hat{\sigma}_n$, where $\hat{\sigma}_n^\dagger = |e_n\rangle\langle g_n|$ and $\hat{\sigma}_n = |g_n\rangle\langle e_n|$ are the raising and lowering operators for the exciton on the n_{th} molecule, respectively. Further, $|g_n\rangle$ and $|e_n\rangle$ are the ground state and excited state of the n_{th} molecule, respectively, $\hbar\omega_{\mathrm{ex}} = E_e - E_g$ is the excitation energy between the ground and excited states, and λ is the reorganization energy (that give rise to Stokes shift in linear spectra) due to exciton-phonon coupling. The $\hat{H}_{\text{ex-b}} + \hat{H}_{\mathrm{b}}$ terms further describe interactions between exciton and phonon bath, with details provided in the Supporting Information.

We model the FP cavity with an open direction x characterized by an in-plane wavevector $k_\parallel$, and one confined direction z where $k_\perp$ is the wavevector of the fundamental mode confined between two cavity mirrors, perpendicular to the mirror surface. The frequencies of the cavity mode are given by

$$\hbar\omega_{\mathbf{k}} = \hbar c\sqrt{k_\parallel^2 + k_\perp^2}, \tag{2}$$

where c is the speed of the light. When $k_\parallel = 0$, $\hbar\omega_{\mathbf{k}}(0) = \hbar c k_\perp \equiv \hbar\omega_{\mathrm{c}}$ is the cavity frequency at normal incidence. The photonic Hamiltonian $\hat{H}_{\mathrm{ph}}$ is expressed as $\hat{H}_{\mathrm{ph}} = \sum_{k_\parallel}\hbar\omega_{\mathbf{k}}(\hat{a}_{\mathbf{k}}^\dagger\hat{a}_{\mathbf{k}} + \frac{1}{2})$, and $\hat{a}_{\mathbf{k}}^\dagger$ and $\hat{a}_{\mathbf{k}}$ are the photonic raising and lowering operators for mode $\mathbf{k}$, respectively. We consider $k_\parallel$ with discrete (but still quasi-continuous) values $k_\alpha = \frac{2\pi}{NL}\alpha$, where the mode indexes $\alpha \in [-\frac{\mathcal{M}-1}{2}, \ldots 0, \ldots \frac{\mathcal{M}-1}{2}]$, and $\mathcal{M} = 283$ is the total number of cavity modes needed to capture the relevant energies for the hybrid system.

The light-matter interaction $\hat{H}_{\mathrm{LM}}$ term is

$$\hat{H}_{\mathrm{LM}} = \sum_{k_\parallel}\sum_{n=0}^{N-1}\hbar g_{\mathbf{k}}\left(\hat{a}_{\mathbf{k}}^\dagger\hat{\sigma}_n e^{-ik_\parallel x_n} + \hat{a}_{\mathbf{k}}\hat{\sigma}_n^\dagger e^{ik_\parallel x_n}\right), \tag{3}$$

where x_n is the location of the n_{th} molecule.[11] Further, the $k_\parallel$-dependent light-matter coupling strength is $g_{\mathbf{k}}(k_\parallel) = g_{\mathrm{c}}\sqrt{\frac{\omega_{\mathbf{k}}}{\omega_{\mathrm{c}}}}\cos\theta$, where g_{c} is the single-molecule light-matter coupling strength at $k_\parallel = 0$ and is chosen as a parameter. A schematic of the model system is provided in Fig. S1 of the Supporting Information. The transport dynamics occur in the single excitation subspace

$$|E_n\rangle = |e_n\rangle\bigotimes_{m\neq n}|g_m\rangle\bigotimes_{k_\parallel\in\{k_\alpha\}}|0_{k_\parallel}\rangle \tag{4a}$$

$$|k_\alpha\rangle = |G\rangle\bigotimes_{k_\parallel\neq k_\alpha}|0_{k_\parallel}\rangle\otimes|1_{k_\alpha}\rangle, \tag{4b}$$

where $|E_n\rangle$ is the singly excited state for the n_{th} molecule located at x_n, $|k_\alpha\rangle$ is the 1-photon-dressed ground state with wave-vector $k_\parallel = k_\alpha$, and $|G\rangle = \bigotimes_n|g_n\rangle\bigotimes_\alpha|0_{k_\alpha}\rangle$ represents the ground state. We assume identical loss rates Γ_{c} for all cavity modes k_α, which is consistent with angle-resolved reflectance measurements of typical FP cavity[17] and previous theoretical work,[7] and define the cavity quality factor at normal incidence ($k_\parallel = 0$) as $\mathcal{Q} = \omega_{\mathrm{c}}/\Gamma_{\mathrm{c}}$.

We use $\mathcal{L}$-MFE dynamics approach[9,10,18] to simulate the polariton transport quantum dynamics in a lossy cavity. This approach describes the exciton-photonic degrees of freedom (DOF) quantum mechanically

$$|\psi(t)\rangle = \sum_{n=0}^{N-1}c_n(t)|E_n\rangle + \sum_\alpha c_\alpha(t)|k_\alpha\rangle \equiv |\psi_{\mathrm{ex}}(t)\rangle + |\psi_{\mathrm{ph}}(t)\rangle. \tag{5}$$

The influence of phonons is computed using the Ehrenfest mixed quantum-classical dynamics, and cavity loss through Lindblad dynamics using a stochastic approach,[9] with details provided in the Supporting Information. The spatial distribution of the polariton is given by $|\psi_{\pm}(x_n,t)|^2 = |\langle \pm, n|\psi(t)\rangle|^2$, with the real space polariton states expressed as

$$|+,n\rangle = \sum_{\alpha}\Big[\sum_{n'=0}^{N-1}\frac{X_{k_\alpha}}{N}e^{ik_\alpha(x_n-x_{n'})}|E_{n'}\rangle + C_{k_\alpha}\frac{e^{ik_\alpha x_n}}{\sqrt{N}}|k_\alpha\rangle\Big], \tag{6a}$$

$$|-,n\rangle = -\sum_{\alpha}\Big[\sum_{n'=0}^{N-1}\frac{C_{k_\alpha}}{N}e^{ik_\alpha(x_n-x_{n'})}|E_{n'}\rangle - X_{k_\alpha}\frac{e^{ik_\alpha x_n}}{\sqrt{N}}|k_\alpha\rangle\Big], \tag{6b}$$

where C_{k_α} and X_{k_α} are the Hopfield coefficients[19] at the in-plane momentum k_α. Detailed derivations are provided in the Supporting Information.

To propagate quantum dynamics, we solve $i\hbar\frac{\partial}{\partial t}|\psi(t)\rangle = \hat{H}_{\mathrm{Q}}(\mathbf{R}(\mathbf{t}))|\psi(\mathbf{t})\rangle$, where $\hat{H}_{\mathrm{Q}} = \hat{H} - \hat{H}_{\mathrm{b}}$ is the quantum part of the Hamiltonian (that include excitonic and photonic DOF). Solving it requires the operation of $\hat{H}_{\mathrm{Q}}$ on $|\psi(t)\rangle$ which is computationally expensive. We develop a novel computational algorithm by realizing that $\hat{H}_{\mathrm{Q}}|\psi\rangle = |\epsilon_\psi\rangle \odot |\psi\rangle + \big(\mathcal{F}^{-1}|\psi_{\mathrm{ex}}\rangle \oplus \mathcal{F}|\psi_{\mathrm{ph}}\rangle\big)$, where the $\odot$ represents a simple Hadamard product between vectors, and $\mathcal{F}$ and $\mathcal{F}^{-1}$ are Fast Fourier Transform (FFT) and inverse FFT, respectively. Further, $|\epsilon_\psi\rangle$ represents a column matrix with the diagonal matrix element of $\hat{H}_{\mathrm{Q}}$, with $|\epsilon_\psi\rangle \equiv [\{\langle E_n|\hat{H}_{\mathrm{Q}}|E_n\rangle\},\{\langle k_\alpha|\hat{H}_{\mathrm{Q}}|k_\alpha\rangle\}]^{\mathrm{T}}$. This algorithm leads to a reduction in computational cost from $\mathcal{O}(N^2)$ to $\mathcal{O}(N\ln N)$) and a nearly 100 times speedup for $N = 10^4$ molecule simulation, see details in the Supporting Information. All results presented in this work are performed under $T = 300$ K.

Fig. 1 illustrates the impacts of reorganization energy λ (in panel b) and cavity loss rate Γ_{c} (in panel c) on polariton group velocities v_g. Here, v_g is computed by following the wavefront of the polariton wavepacket, using the method outlined in Ref. 3, with details provided in the Supporting Information.

Fig. 1a presents the energy diagrams for the UP and LP bands formed from hybridizing the photonic band and the excitonic band. The LP and UP bands are color-coded based on their photonic character. The collective light-matter coupling strength is $\sqrt{N}g_{\mathrm{c}} = 120$ meV. These polariton states are analytically expressed in Eq. S13 in the Supporting Information. The initial excitation conditions are indicated in Fig. 1 using black dots on the LP branch, corresponding to a pulse with a narrow energy bandwidth (to model the experimental condition in Ref. 3).

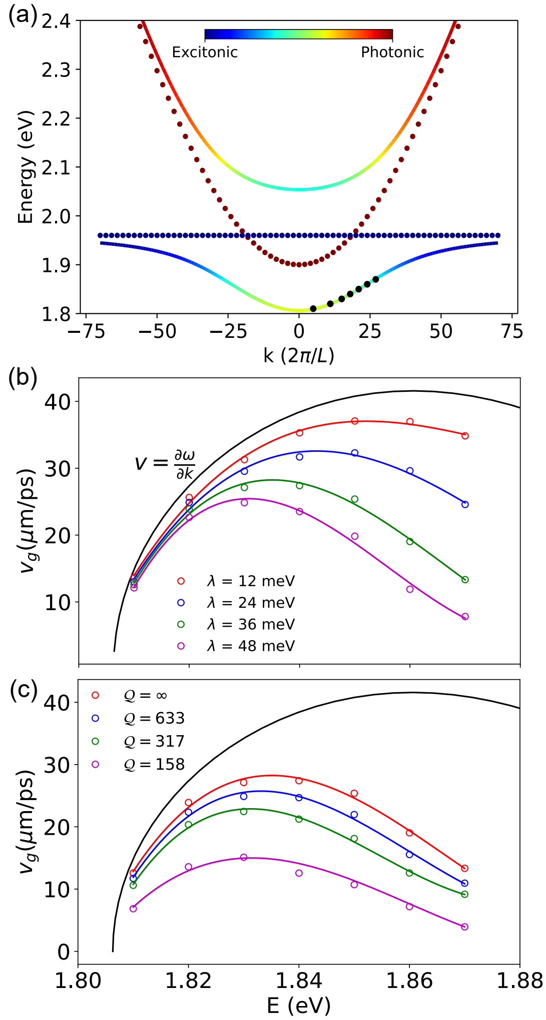

Figure 1: **Energy-resolved investigation of dissipative effects on polariton group velocity.** (**a**) Dispersion curve of the photon (red dots) and matter (blue dots) (**b**) Group velocities v_g of polaritons for various reorganization energy λ in a lossless cavity. (**c**) Group velocities v_g of polaritons for different cavity quality factor $\mathcal{Q}$ with phonon reorganization energy $\lambda = 36$ meV.

Fig. 1b shows v_g with different initial energies (corresponding to different $k_{\parallel}$ in Fig. 1a). Here, the cavity is lossless, with $\Gamma_{\mathrm{c}} = 0$. The solid black line indicates the group velocity obtained as $v_g = \partial\omega_-/\partial k_{\parallel}$. The open circles with different colors are v_g for the excitonic system with different reorganization energy λ. As λ increases, v_g decreases, indicating that the polaritons propagate at a reduced v_g due to increased exciton-phonon coupling, which was referred to as the group velocity renormalization.[3] Increasing λ or increasing

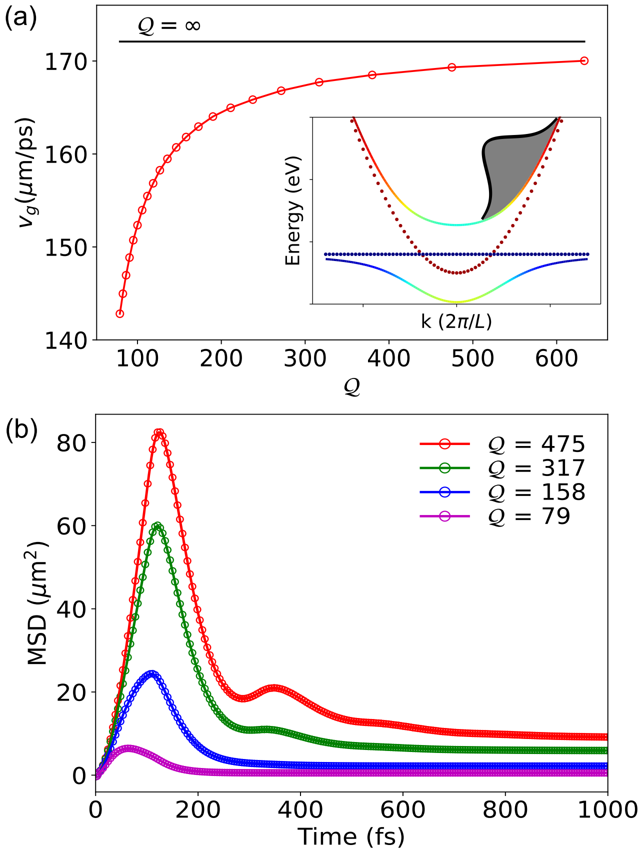

Figure 2: **Group velocity dependence on quality-factor for UP broadband excitation.** (**a**) Polariton group velocity v_g vs cavity quality factor $\mathcal{Q}$. The inset figure shows the energy bandwidth used for the initial excitation in the UP branch, optimizing the localization of the polariton wavepacket. Results are converged with 250 trajectories, validated against a set of runs with 1000 trajectories. (**b**) Time-dependent transient MSD with UP initial excitation for various $\mathcal{Q}$.

the excitonic character (increasing E) causes more renormalization of v_g, in agreement with the results in Ref. 3. Fig. 1c illustrates the effects of cavity loss on v_g by changing the $\mathcal{Q}$ factor (loss rate Γ_c), with fixed $\lambda = 36$ meV. With a decreasing $\mathcal{Q}$ (increasing Γ_c), v_g further decreases due to rapid attenuation of the photonic contribution to the polariton wavepacket.

Fig. 2a presents the impact of cavity quality factor $\mathcal{Q}$ on v_g with a broadband excitation on the UP band (indicated with the gray Gaussian wavepacket in the inset of Fig. 2a), to model similar experimental conditions in Ref. 2. Here, we use $\lambda = 36$ meV and vary the $\mathcal{Q}$ factor. As shown in Fig. 2, v_g increases with increasing $\mathcal{Q}$. Our results demonstrate a trend consistent with experimental measurements in Ref. 2 (see Fig. 2e of that work).

Fig. 2b presents the transient MSD $\sigma^2(t)$ of a polariton wavepacket under various $\mathcal{Q}$-factors, which is computed as[7,20]

$$\sigma^2(t) = \langle\psi(t)|(\hat{x} - \langle x\rangle)^2|\psi(t)\rangle, \tag{7}$$

where $\langle x\rangle$ is the centroid of the initial polariton wavepacket (at $t = 0$) in position space. In a very lossy cavity $\mathcal{Q} = 79$ (magenta curve), the wavepacket shows minimal spread within a brief duration of time for $t \sim 50$ fs), and its MSD returns to its initial value after a long time (∼1 ps). With an increase in $\mathcal{Q}$, both the wavepacket's maximum MSD and the corresponding rise time increase. The initial rise of MSD is again attributed to the polariton's photonic character, which is responsible for ballistic transport, as pointed out in recent theoretical work.[7] The dip in MSD right after the initial rise is attributed to both the decay of the UP population to the dark states, and to cavity loss, which are competing at a similar time scale, with details provided in Fig. 3. We note that the steady-state MSD in lossy cavities with $\mathcal{Q} > 158$ surpasses the MSD of the original polariton wavepacket at t=0, suggesting that strong light-matter coupling (here, $\sqrt{N}g_c = 120$ meV) facilitates the expansion of the underlying excitons over a larger volume even in the presence of cavity loss. The observed trends in our numerical simulations are consistent with transient absorption spectral measurements (see Fig. 2c in Ref. 2). Similar studies where the LP branch is excited are reported in the Supporting Information, and we observe a similar trend for the transient MSD but no corresponding rise and dip.

Fig. 3a and Fig. 3b present the population dynamics of the UP (blue), LP (red), and dark states (black) under broadband UP excitation and broadband LP excitations respectively, with cavity quality factors of $\mathcal{Q} = 475$. The ground-state population (green) is also depicted. For N molecules and $\mathcal{M}$ cavity modes, there is a total of $\mathcal{M}$ different UP states (with different k_α), $\mathcal{M}$ different LP states, and $N - \mathcal{M}$ dark exciton states. The definitions of UP, LP, and Dark states are provided in Eqs. S12-13 of the Supporting Information. Here, we group the same type of states together to visualize the transitions among these manifolds of states.

In Fig. 3a, an initial substantial decrease in the UP population is observed, accompanied by a sharp increase in the dark state population and a slower rate of increase in the ground state population. The population transfer from the UP to the dark state is mediated by exciton-phonon

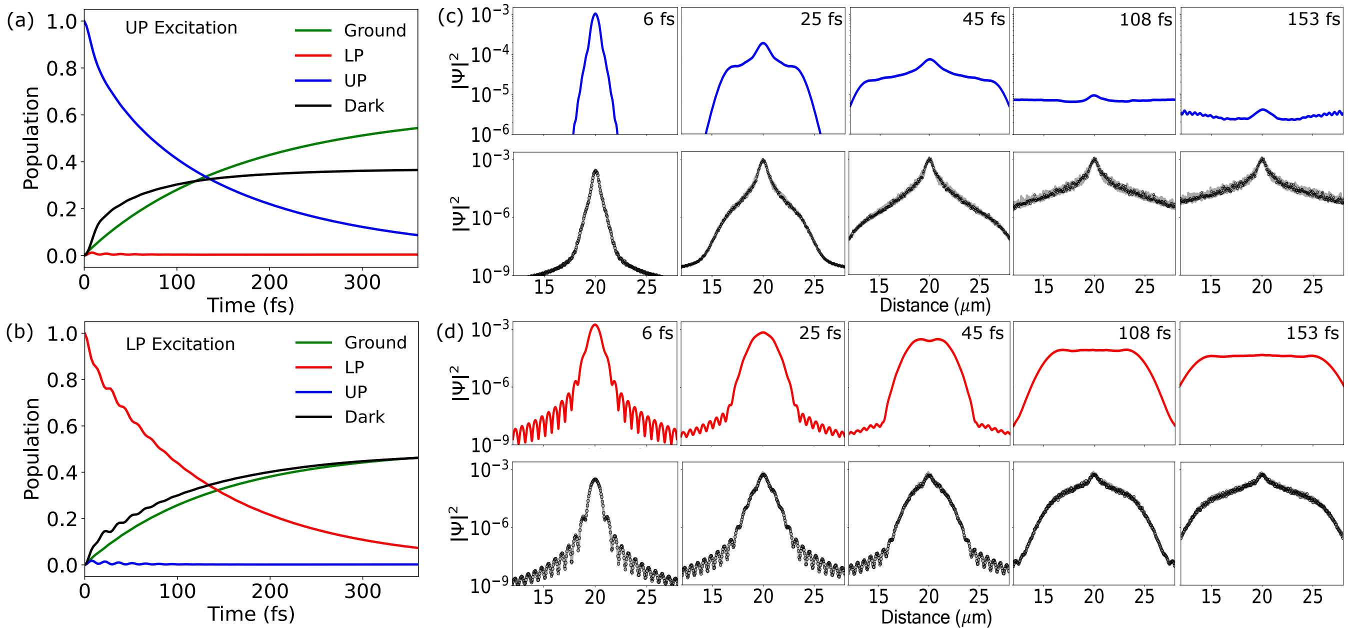

Figure 3: **Polariton population dynamics and wavepacket.** The populations of UP (blue), LP (red), dark (black), and ground states (green) in a cavity with $\mathcal{Q} = 475$ are presented, with (**a**) broadband UP excitation and (**b**) broadband LP excitation. The wavepackets in position space, decomposed into polariton and dark state components, are illustrated for (**c**) broadband UP excitation and for (**d**) broadband LP excitation.

coupling,[21,22] and the population transfer to the ground state is attributed to cavity loss. Here, with a high $\mathcal{Q}$, it is evident that exciton-phonon coupling has more influence on the decay of the initial UP population than cavity loss. For a broadband LP excitation shown in Fig. 3b, an initial substantial decrease in the LP population is observed, and the rate of population transfer from LP to the ground state is similar to the rate of population transfer from LP to the dark states.

Fig. 3c and Fig. 3d present the polariton wavepacket and the dark exciton density in position space for broadband excitations. Over time, the UP (blue) and LP wavepacket (red) propagates outward from the center, primarily due to their *photonic character* which exhibit ballistic transport (with v_g largely adopted from the derivative of the band). Due to the exciton-phonon coupling, the UP and LP wavepackets transfer population to the dark state, resulting in an increase in the dark state (black) probability densities. The resultant dark-state wavepacket is largely immobile, as it consists of excitons that move diffusively in most transport experiments. In current theoretical studies, these dark states are completely immobile because of their dispersionless band assumed in the model (Fig. 1a). However, we note that in some materials, even exciton exhibits wavelike transport at room temperature,[23] and the role of the dark states need to be carefully examined for those materials when coupling them inside the cavity.

Due to the larger v_g of the UP wavepacket, the polariton wavepacket expands rapidly in early time, contributing to a sharp rise in the total transient MSD (Fig 2b). As the UP expands, it also transfers populations to the dark exciton states (at the location of x_n which UP is visiting), but with a slower transfer speed compared to v_g. Consequently, the UP wavepacket (blue curve in Fig. 3c) propagates more rapidly than the dark state wavepacket (black curve in Fig. 3c). Note that the dark exciton in our model has $v_g = 0$ from the derivative of the dispersion curve. The effective propagation of the dark exciton wavepacket is only due to the transfer of population from UP which propagates ballistically in space at an early time. After $t = 108$ fs, the UP wavepacket is further spread out and its amplitude also starts to decrease due to cavity loss, resulting in a decrease in its magnitude, as well as its contribution to the transient MSD. In addition, the interference term for UP excitation is constructive, further adding to the contribution of transient MSD at an early time. This constructive interference is fragile to decoherence and eventually disappears after a long time. Thus, a faster v_g in the UP band, a relatively slow UP to dark state transition rate, and constructive interference between exciton and photon wavepacket, together explain the MSD behavior as shown in Fig. 2b, where the MSD initially increases to a peak value before declining.

In contrast, for the LP wavepacket, Fig. 3d shows a more gradual expansion of the polariton wavepacket. For instance, at $t = 45$ fs, the LP wavepacket (red curves) spans a width ranging from about 18 μm to 22 μm only, which is similar to the width of the corresponding dark-state wavepacket at $t = 45$ fs. This is because the LP wavepacket advances at a rate comparable to the rate of LP to dark state transition, resulting in a synchronized expansion of both LP and dark exciton wavepacket. In addition, the interference contribution for MSD is destructive, which further reduces the transient MSD (see Fig. S3 in Supporting Information).

We investigate the behavior of polariton transport due to the influence of the photonic character of the initial wave packet at $t = 0$. We consider $\lambda = 36$ meV, and $\mathcal{Q} = 633$ (which is in line with the cavity used in Ref. 1), and a narrow band of initial excitation conditions with a narrow range of $k_{\parallel}$ on the LP state (see Fig. 1a), to model the k-selective probing conditions in Ref. 3 and Ref. 1. Here, we consider a cavity with a lower frequency for this study ($\hbar\omega_c = 1.77$ eV at $k_{\parallel} = 0$), which is more red-detuned compared to the curve presented in Fig. 1a. For each initial excitation condition with a given $k_{\parallel}$, we report the corresponding photonic characters $|\chi_{\rm ph}|^2 = \sum_\alpha |c_\alpha(t = 0)|^2$ of the wavepacket, defined as the sum of the photonic components of the polariton at $t = 0$. To determine the transport characteristics, we perform a least-square fitting of the transient MSD with the equation

$$\sigma^2(t) = \sigma^2(t_0) + D \cdot t^\gamma, \tag{8}$$

which corresponds to a generalized diffusion equation.[1,24] The constant D represents the generalized diffusion coefficient, while the exponent γ characterizes the transport properties. For $\gamma = 1$, the transport is diffusive, for $\gamma = 2$, the transport is ballistic,[1,3] and for $\gamma < 1$, the transport is subdiffusive.[25]

Fig. 4a presents the time-dependent MSD (Eq. 7). We find that there are two separate transport stages, one at early times with $\gamma \approx 2$ (with black solid lines as the fitting lines) and one at later times, with $\gamma \approx 1$ (red solid lines as fitting lines). Fig. 4b provides the value of γ as a function of $|\chi_{\rm ph}|^2$, obtained from the fitting in panel (a).

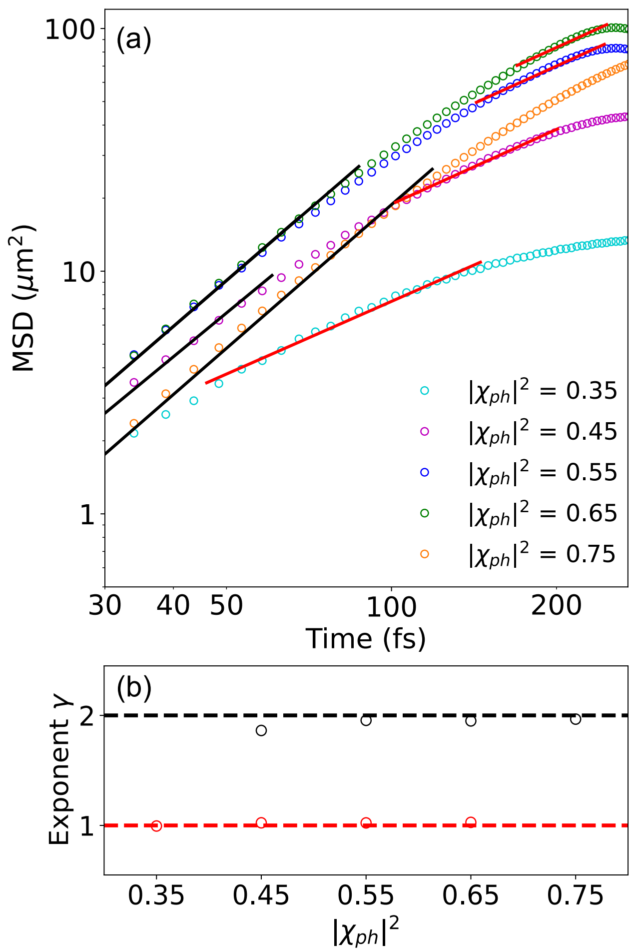

Figure 4: **A transition from ballistic to the diffusive transport.** (**a**) MSD for the polariton as a function of time, with various photonic character $|\chi_{\rm ph}|^2$. (**b**) The exponents extracted from fitting the MSDs with various photonic character $|\chi_{\rm ph}|^2$ with Eq. (8).

The duration of the ballistic stage depends on the photonic character of the wavepacket at $t = 0$. For small photonic characters ($|\chi_{\rm ph}|^2 = 0.45$), the ballistic stage lasts for up to 50 fs while for large photonic characters ($|\chi_{\rm ph}|^2 = 0.75$), the ballistic stage lasts for a longer duration of up to 100 fs. Further, the wavepacket transitions from purely ballistic ($|\chi_{\rm ph}|^2 = 0.75$) to purely diffusive ($|\chi_{\rm ph}|^2 = 0.35$) transport as $|\chi_{\rm ph}|^2$ decreases. This suggests that for the initial polariton wavepacket, the transport is ballistic for a duration (with v_g being renormalized by exciton-phonon coupling and cavity loss), before gradually becoming diffusive. This observation is in close agreement with recent experiments (*e.g.*, Fig. 2c in Ref. 3 and Fig. 4 in Ref. 1).

Note that even under the diffusive transport stage ($\gamma \approx 1$) the group velocity is still much larger than the expected gradient of matter dispersion (which is 0 in the current model). Also, the absolute value of MSD depends on the group velocity, and with a large photonic contribution $|\chi_{\rm ph}|^2 = 0.75$, the gradient of the LP dispersion is relatively small (close to a small $k_\parallel$ value in FP cavity as indicated in Fig. 1a). As such, for $|\chi_{\rm ph}|^2 = 0.75$, even though the transport is ballistic for the longest time (for $t < 100$ fs) compared to the other cases investigated here, the MSD is not necessarily the largest.

We developed an efficient approach for investigating polariton transport with quantum dynamics simulations. We achieved quasi-linear scaling for our quantum dynamical method, enabling simulations of $N = 10^4$ molecules collectively coupled to $\mathcal{M} = 10^2$ cavity modes in a GHTC Hamiltonian. The results from quantum dynamics simulations confirm the v_g renormalization effects[1,3] and demonstrate the v_g reduction due to exciton-phonon coupling and cavity loss. Furthermore, the transient MSD of polariton wavepackets with broadband UP excitation demonstrates transient growth and then contraction, agreeing with the experimental observations in Ref. 2. This is due to fast expansion of the UP polariton wavepacket in space and the relatively slower rate of transitions to the dark exciton wavepacket, as demonstrated by our quantum dynamics analysis (Fig. 3). Finally, from the transient MSD, we were able to analyze the transport characteristics of the wavepacket that illustrates a ballistic-to-diffusive turnover, which has been experimentally observed in Ref. 3 and Ref. 1. Overall, the results from our quantum dynamics simulations successfully capture all the trends observed in recent polariton transport experiments.[1–3] The current theory does not consider static disorders,[26,27] inter-molecular interactions, or Peierls phonon (that fluctuates the inter-site couplings). Their influence will be explored in future work.

Supporting Information. Details of Model Hamiltonian; Polariton Quantum Dynamics Propagation Method; Details of Quantum Dynamics Simulations; Details of Polariton Transport Properties Calculations; Additional Numerical Results.

Acknowledgement This work was supported by internal funding from the University of Rochester. Computational resources were provided by the Center for Integrated Research Computing (CIRC) at the University of Rochester. The authors thank Mike Taylor for making the TOC Figure. The authors appreciate valuable discussions and comments from Eric Koessler, Braden Weight, Arkajit Mandal, and Michael Taylor. P. H. appreciates valuable discussions with Andrew Musser, Tal Schwartz, and Milan Delor. P.H. appreciates the mechanism of polariton propagation dragging the dark exciton expansion which was pointed out by Milan Delor through private communications.

References

(1) Balasubrahmaniyam, M.; Simkhovich, A.; Golombek, A.; Sandik, G.; Ankonina, G.; Schwartz, T. From enhanced diffusion to ultrafast ballistic motion of hybrid light–matter excitations. *Nature Materials* **2023**, *22*, 338–344.

(2) Pandya, R.; Ashoka, A.; Georgiou, K.; Sung, J.; Jayaprakash, R.; Renken, S.; Gai, L.; Shen, Z.; Rao, A.; Musser, A. J. Tuning the coherent propagation of organic exciton-polaritons through dark state delocalization. *Advanced Science* **2022**, *9*, 2105569.

(3) Xu, D.; Mandal, A.; Baxter, J. M.; Cheng, S.-W.; Lee, I.; Su, H.; Liu, S.; Reichman, D. R.; Delor, M. Ultrafast imaging of polariton propagation and interactions. *Nature Communications* **2023**, *14*, 3881.

(4) Jin, L.; Sample, A. D.; Sun, D.; Gao, Y.; Deng, S.; Li, R.; Dou, L.; Odom, T. W.; Huang, L. Enhanced two-dimensional exciton propagation via strong light–matter coupling with surface lattice plasmons. *ACS Photonics* **2023**, *10*, 1983–1991.

(5) Berghuis, A. M.; Tichauer, R. H.; de Jong, L. M.; Sokolovskii, I.; Bai, P.; Ramezani, M.; Murai, S.; Groenhof, G.; Gómez Rivas, J. Controlling exciton propagation in organic crystals through strong coupling to plasmonic nanoparticle arrays. *ACS photonics* **2022**, *9*, 2263–2272.

(6) Rozenman, G. G.; Akulov, K.; Golombek, A.; Schwartz, T. Long-range transport of organic exciton-polaritons revealed by ultrafast microscopy. *ACS photonics* **2018**, *5*, 105–110.

(7) Tichauer, R. H.; Sokolovskii, I.; Groenhof, G. Tuning the Coherent Propagation of Organic Exciton-Polaritons through the Cavity Q-factor. *Advanced Science* **2023**, *10*, 2302650.

(8) Chng, B. X.; Ying, W.; Lai, Y.; Vamivakas, A. N.; Cundiff, S. T.; Krauss, T. D.; Huo, P. Mechanism of Molecular Polariton Decoherence in the Collective Light–Matter Couplings Regime. *The Journal of Physical Chemistry Letters* **2024**, *15*, 11773–11783.

(9) Koessler, E. R.; Mandal, A.; Huo, P. Incorporating Lindblad decay dynamics into mixed quantum-classical simulations. *The Journal of Chemical Physics* **2022**, *157*, 064101.

(10) Hu, D.; Chng, B.; Ying, W.; Huo, P. Trajectory-based Non-adiabatic Simulations of the Polariton Relaxation Dynamics. *ChemRxiv* **2024**, 10.26434/chemrxiv–2024–t818f.

(11) Mandal, A.; Taylor, M. A.; Weight, B. M.; Koessler, E. R.; Li, X.; Huo, P. Theoretical advances in polariton chemistry and molecular cavity quantum electrodynamics. *Chemical Reviews* **2023**, *123*, 9786–9879.

(12) Tichauer, R. H.; Feist, J.; Groenhof, G. Multi-scale dynamics simulations of molecular polaritons: The effect of multiple cavity modes on polariton relaxation. *The Journal of Chemical Physics* **2021**, *154*, 104112.

(13) Taylor, M.; Mandal, A.; Huo, P. Light-Matter Interaction Hamiltonians in Cavity Quantum Electrodynamics. *ChemRxiv* **2024**, 10.26434/chemrxiv–2024–dklxd.

(14) Mandal, A.; Xu, D.; Mahajan, A.; Lee, J.; Delor, M.; Reichman, D. R. Microscopic theory of multimode polariton dispersion in multilayered materials. *Nano Letters* **2023**, *23*, 4082–4089.

(15) Taylor, M. A.; Weight, B. M.; Huo, P. Reciprocal asymptotically decoupled Hamiltonian for cavity quantum electrodynamics. *Physical Review B* **2024**, *109*, 104305.

(16) Li, J.; Golez, D.; Mazza, G.; Millis, A. J.; Georges, A.; Eckstein, M. Electromagnetic coupling in tight-binding models for strongly correlated light and matter. *Physical Review B* **2020**, *101*, 205140.

(17) Qiu, L.; Mandal, A.; Morshed, O.; Meidenbauer, M. T.; Girten, W.; Huo, P.; Vamivakas, A. N.; Krauss, T. D. Molecular polaritons generated from strong coupling between CdSe nanoplatelets and a dielectric optical cavity. *The Journal of Physical Chemistry Letters* **2021**, *12*, 5030–5038.

(18) Mondal, M. E.; Koessler, E. R.; Provazza, J.; Vamivakas, A. N.; Cundiff, S. T.; Krauss, T. D.; Huo, P. Quantum dynamics simulations of the 2D spectroscopy for exciton polaritons. *The Journal of Chemical Physics* **2023**, *159*, 094102.

(19) Deng, H.; Haug, H.; Yamamoto, Y. Exciton-polariton bose-einstein condensation. *Reviews of modern physics* **2010**, *82*, 1489.

(20) Aroeira, G. J.; Kairys, K. T.; Ribeiro, R. F. Coherent transient exciton transport in disordered polaritonic wires. *Nanophotonics* **2024**, *13*, 2553–2564.

(21) Ying, W.; Mondal, M. E.; Huo, P. Theory and quantum dynamics simulations of exciton-polariton motional narrowing. *The Journal of Chemical Physics* **2024**, *161*, 064105.

(22) Lai, Y.; Ying, W.; Huo, P. Non-Equilibrium Rate Theory for Polariton Relaxation Dynamics. *The Journal of Chemical Physics* **2024**, *161*, 104109.

(23) Tulyagankhodjaev, J. A.; Shih, P.; Yu, J.; Russell, J. C.; Chica, D. G.; Reynoso, M. E.; Su, H.; Stenor, A. C.; Roy, X.; Berkelbac, T. C.; Delor, M. Room-temperature wavelike exciton transport in a van der Waals superatomic semiconductor. *Science* **2023**, *382*, 438–442.

(24) Klafter, J.; Sokolov, I. M. *First steps in random walks: from tools to applications*; OUP Oxford, 2011.

(25) Delor, M.; Weaver, H. L.; Yu, Q.; Ginsberg, N. S. Imaging material functionality through three-dimensional nanoscale tracking of energy flow. *Nature materials* **2020**, *19*, 56–62.

(26) Engelhardt, G.; Cao, J. Polariton Localization and Dispersion Properties of Disordered Quantum Emitters in Multimode Microcavities. *Phys. Rev. Lett.* **2023**, *130*, 213602.

(27) Tutunnikov, I.; Qutubuddin, M.; Sadeghpour, H. R.; Cao, J. Characterization of Polariton Dynamics in a Multimode Cavity: Noise-enhanced Ballistic Expansion. 2024; https://arxiv.org/abs/2410.11051.

Figure 5: TOC Graphic